A&A 365, 186–197 (2001)
DOI: 10.1051/0004-6361:20000016

Astronomy & Astrophysics

Properties of EUV and X-ray emission in solar active regions

S. A. Matthews[1], J. A. Klimchuk[2], and L. K. Harra[1]

[1] Mullard Space Science Laboratory, University College London, Holmbury St. Mary, Surrey RH5 6NT, UK
[2] Space Science Division, Code 7675, Naval Research Laboratory, Washington, DC 20375-5352, USA

Received 9 November 1999 / Accepted 5 October 2000

Abstract. Using observations from the Coronal Diagnostic Spectrometer (CDS) on SoHO and the Soft X-ray Telescope (SXT) on Yohkoh we investigate how the spatial properties of active region emission observed in the EUV and X-ray range varies with temperature. We examine the contrast per unit area of the EUV emission from a number of active regions, and employ correlation techniques and Fourier methods with which we obtain the two dimensional power spectrum of the intensity distribution for a number of images in emission lines formed at different temperatures. Integrating this over polar angle we find isotropic power-law behaviour at all temperatures in a number of topologically different active regions, with a tendency for flatter spectra at lower temperatures. The existence of power-law spectra indicates that there is no preferred length scale within the regions, at least not a resolvable one, while flatter spectra at lower temperatures indicate that the structures are relatively smaller in this temperature range, possibly providing support for the idea of a multi-component transition region (TR). Implications for various heating models are discussed.

Key words. Sun: UV radiation – Sun: Corona – Sun: transition region

1. Introduction

Observations from Skylab showed us that the outer atmosphere of the Sun is in fact much more highly structured than had previously been imagined. The distribution of the EUV and X-ray emission observed in these outer regions is determined in part by the magnetic field, which allows plasma and thermal energy to flow preferentially in the direction of the field lines, and in part by spatial nonuniformities of the heating rate, which causes some field lines to "light up" more than others. A review of the Skylab active region observations (e.g. Cheng 1980; Cheng et al. 1980; Dere 1980; Sheeley 1980; Mariska et al. 1980) was given by Webb (1981) in which he concluded several points regarding the classification of active region loops. Firstly, the observations seemed to indicate that the number of complete, identifiable loops increases with increasing temperature of the line in which the region is viewed. Secondly, hot loops and cool transition region loops are not co-spatial and have quite different physical characteristics, and thirdly that the brightest hot loops form low-lying arcades crossing the magnetic neutral line, often with the loops ending in sunspot penumbrae. He suggested that from the observations available there were at least two classes of loops; cool umbral loops and relatively stable hot loops with the possible existence of an intermediate class of transient, nonumbral cool loops. Due to their transient nature these were infrequently observed.

Since Skylab there has been no significant opportunity to study the distribution of emission in active regions over a wide temperature range, although a number of recent rocket observations carried out in coordination with Yohkoh (e.g. Solar EUV Rocket Telescope (SERTS) and High Resolution Telescope and Spectrograph (HRTS)) have investigated the structure of active regions from the low transition region to corona. Strong & Bruner (1996) summarized the results of the various rocket experiments and found that while the cool plasma outlines the coronal legs, the hot plasma shows the apex of the coronal loops. However, they observed low temperature plasma extending into the corona. Emission from the C IV line in the form of loops was observed by Athay et al. (1983) with the Solar Maximum Mission (SMM). A study of these loops showed that their scale heights were more consistent with coronal temperatures than with the emission from 1 10^5 K plasma expected, and it was concluded that they were the result of rapid cooling of coronal loops (Strong & Bruner 1996). Brosius et al. (1997) presented a detailed study of 2 active regions observed with SERTS and SXT. They found that the intensity from Fe XV and Fe XVI lines closely follows the soft X-ray emission observed by SXT. However, the emission from the He II and Mg IX lines formed at cooler temperatures tends to exist at the loop footpoints, as well as at structures removed from the hot loops. Recent observations from TRACE have revealed a bright low-lying emission in the Fe IX/Fe X 171 Å band called moss (Berger et al. 1999). This emission from plasma at

Send offprint requests to: S. A. Matthews

approximately 1 MK appears to delineate the footpoints of hot coronal loops visible with SXT at temperatures of between 3–5 MK and it has been suggested that it is in fact the classical conductively heated upper transition region (Martens et al. 1999). Poor correlation is found between the moss and magnetic elements visible in magnetograms and Ca II K line emission, supporting the picture of coronal loops being formed by the merging or tangling of field lines.

The wealth of observations from the Solar and Heliospheric Observatory (SoHO) in the EUV range provide us with the opportunity to further our knowledge of the structure of active regions. These observations, and in particular those from CDS, represent a significant resource of active region data offering in many cases simultaneous temperature coverage from $10^4 - > 10^6$ K. To date, CDS has reinforced the Skylab results that there is very little spatial correspondence between hot and cool emission but that often low temperature plasma extends to similar heights (e.g. Matthews & Harra-Murnion 1997; Fludra et al. 1997). Recent observations by Nagata et al. (1999) using the XUV Doppler Telescope, Extreme Ultraviolet Imaging Telescope (EIT) and Yohkoh SXT also confirm this general lack of correspondence between 1–2 MK and >2.5 MK loops.

The central aim of this paper is to use CDS observations to try to establish the connection, if any, between the structures observed at different temperatures in active regions. Are differences in the spatial distribution of the emission also indicative of differences in heating and is this consistent with the other observed active region properties at different temperatures?

We attempt to search for quantitative differences between emission that falls into the cool (< 1 MK) and hot (> 1 MK) classes by examining the spatial distribution of different temperature emission in the following ways: the behaviour of intensity correlations between images formed in different temperature lines; the contrast between the loop and background emission; and searching for evidence of different characteristic spatial scales with temperature. We apply similar Fourier methods to those used by Gomez et al. (1993) and Martens & Gomez (1992) to obtain 2-D power spectra of the emission at different temperatures and integrate these over polar angle to obtain the omni-directional power spectra to search for evidence of characteristic size scales.

2. Observations

In this work we have used data from six active regions observed on twelve different days. Four regions were observed only once; one was observed twice; and one was observed six times during its disk passage. The data were obtained by the CDS instrument on SoHO. CDS consists of two spectrometers (the Normal Incidence Spectrometer (NIS) and the Grazing Incidence Spectrometer (GIS)) covering the wavelength range from 151–785 Å and is described in detail by Harrison et al. (1995). The observations presented here were obtained by the NIS which is stigmatic and covers two wavelength ranges: 308–381 Å and 513–633 Å. All of our studies include a wide range of lines formed at different plasma temperatures ranging from the O III 599 Å line ($T_{\max} \simeq 10^5$ K) to the Fe XVI 360 Å line with a temperature of peak formation of $\simeq 2.25\ 10^6$ K for observations on the disk. The limb studies which we use to examine the contrast also include the He I 584 Å and Mg IX 368 Å lines. For three active regions on the disk (NOAA AR 8122, 8227 and 7973) we also have data from the Al.1 and AlMg filters of the SXT on Yohkoh. All of the NIS studies were performed using the $2'' \times 240''$ slit, with a pixel resolution of $2.04'' \times 1.67''$ in solar x and y. The point spread function of NIS has been derived from a comparison of intercalibration data with the SUMER (Solar UV Measurement of Emitted Radiation) instrument also on SOHO by Pauluhn et al. (1999) using the NIS $4''$ slit. They found $FWHM\ (x) = 6''$ and $FWHM\ (y) = 8''$, but suggested that slightly better spatial resolution in the x direction was likely with the $2''$ slit. Standard calibration procedures were applied to both the NIS and SXT data. We obtained temperatures for the SXT observations using filter ratios (Hara 1996); these were in the range 2.4–3.9 MK. The CDS raster number, NOAA AR number, position relative to Sun centre and date of the observations are listed in Table 1, and Table 2 gives a list of the

Table 1. Details of the observed active regions

CDS Exp.	NOAA AR	Posn. ($''$)	Date
s3214	7973	(−1014, 154)	19 Jun. 96
s3260	7973	(−370, 130)	23 Jun. 96
s3817	7981	(−942, −137)	27 Jul. 96
s6711	8011	(10,0)	17 Jan. 97
s9899	8114	(430, −498)	6 Dec. 97
s9903	8114	(507, −483)	7 Dec. 97
s9916	8114	(653, −485)	8 Dec. 97
s9934	8114	(805, −485)	9 Dec. 97
s9943	8114	(836, −485)	10 Dec. 97
s9950	8114	(866, −484)	11 Dec. 97
s9962	8122	(144, 507)	12 Dec. 97
s11297	8227	(−53, 420)	30 May 98

Table 2. Temperatures of peak formation for observed emission lines

Line	Wavelength (Å)	Temperature (K)
He I	584.30	$4.0\ 10^4$
O III	599.59	$1.0\ 10^5$
O IV	554.51	$1.8\ 10^5$
O V	629.73	$2.24\ 10^5$
Ne VI	562.83	$3.98\ 10^5$
Si VIII	319.82	$7.94\ 10^5$
Mg IX	368.06	$8.90\ 10^5$
Mg X	624.95	$1.12\ 10^6$
Si XII	520.67	$1.78\ 10^6$
Fe XIV	334.17	$1.78\ 10^6$
Fe XVI	360.78	$2.24\ 10^6$

lines used in this study together with their temperature of peak formation in ionization equilibrium.

3. Analysis and results

3.1. Intensity correlations with temperature

In order to examine the relationship between the spatial distribution of intensity in the active region images we first fitted the spectrum in each pixel of the image to produce an intensity map in each line. Examples of both a disk and a limb active region are shown in Figs. 1 and 2. The intensity scaling is linear. For three active regions, including that in Fig. 1, we computed the correlation coefficient between each map and the map formed by the line next lowest in temperature. We also investigated the relationship of each image to that formed in the lowest temperature line in our disk studies, O III ($T_{\max} = 10^5$ K).

Since there is considerable uncertainty in interpreting the statistical significance of a linear correlation coefficient, we chose instead to use nonparametric methods which are more robust and involve replacing the actual values in the distribution with their ranks. We used Spearman's rank order correlation coefficient (Press et al. 1992), $r_{\rm s}$. For N measurements (x_i, y_i) we let R_i be the rank of x_i among the other x's, and S_i be the rank of y_i among the other y's. Then the rank-order correlation coefficient, $r_{\rm s}$, is defined to be the linear correlation coefficient of the ranks, i.e.

$$r_{\rm s} = \frac{\sum_i (R_i - \bar{R})(S_i - \bar{S})}{\sqrt{\sum_i (R_i - \bar{R})^2}\sqrt{\sum_i (S_i - \bar{S})^2}}.$$

The significance of a non-zero value of $r_{\rm s}$ can be tested by computing $t = r_{\rm s}\sqrt{\frac{N-2}{1-r_{\rm s}^2}}$, which is distributed approximately as a Student's t distribution with $N-2$ degrees of freedom. The probabilities of obtaining $r_{\rm s} = 0.4$ and 0.9 from random data are 1.1 10^{-3} and 4.89 10^{-24}, respectively. At $r_{\rm s} = 0.2$ the probability rises to 10%. For each of our image pairs we computed $r_{\rm s}$ and plotted this against temperature. Figure 3 shows the variation of the adjacent correlation coefficient with temperature, while Fig. 4 shows it relative to O III.

We found that for all of the active regions on disk that we studied the correlation showed similar behaviour. In the adjacent case the correlation coefficient at first remains nearly constant at a value close to 1 and then falls sharply to a minimum near $\log T = 5.8$. It then rises again to a high value which is close to that at lower temperatures.

For the correlation of images relative to the coolest O III line we again found that the trend was the same for all the active regions studied. The correlation is close to one for low temperatures falling steeply to give a minimum at approximately $\log T = 5.8$. However, instead of rising again to a high value like the adjacent correlation, the value of the coefficient remains mostly weak relative to O III for $\log T > 5.8$.

Both correlation analyses lead us to the same conclusion: the emissions from plasma cooler than about 4 10^5 K are spatially well correlated, as are the emissions from plasma hotter than about 8 10^5 K, but the differences between these two temperature regimes are large.

3.2. Disk to limb variation

We then searched for variations in the behaviour of the intensity correlations described above with position of the active region on the disk. Active region NOAA 8114 was observed daily throughout its passage from the central meridian to the West limb in December 1997 and the intensity correlation coefficients calculated on each day. In Figs. 5 and 6 we have plotted the average value of the correlation coefficient for the adjacent case and that relative to the O III line respectively. The different symbols represent the times when the active region was well onto the disk ((×), position from sun centre in arcsec: (430, −498), (507, −483), (653, −485)) and when it was approaching the limb ((⋄), position from sun centre in arcsec: (805, −485), (836, −485), (866, −484)). The error bars represent the standard deviation from this average value for each case. It can be seen that while the trend remains the same for both these cases, the standard deviations for the case relative to O III approaching the limb are somewhat larger than for the on disk case. The spatial correlation between the hot and cool plasma emission decreases toward the limb, possibly because the hot and cool plasmas have an approximate vertical alignment, with the cooler plasma residing at a generally lower altitude.

3.3. Loop contrast with temperature

When looking at images of active regions formed at different temperatures there is an indication that those structures observed at lower temperatures have a greater contrast than those at higher temperatures (e.g. Fig. 2). In order to quantify this apparent difference we calculated the contrast of the emission of observed structures in the active region to the background emission. For regions on the limb we selected a region encompassing the active region emission above the limb, but excluding the bright limb emission, which would obviously lead to erroneously large contrast values. By doing this we necessarily exclude the emission from the active region at and just inside the limb. However, we believe that since cool loops are best observed above the limb a study of the contrast here is still useful. The active region structures were then defined to be those pixels which had $I > \bar{I}$, and the background those pixels with $I \leq \bar{I}$, where $\bar{I}$ is the average intensity in the selected region of the raster (above and excluding the limb). On the disk we used the whole raster to include both active region and background emission. In both cases the area defined was the same area used for all the images

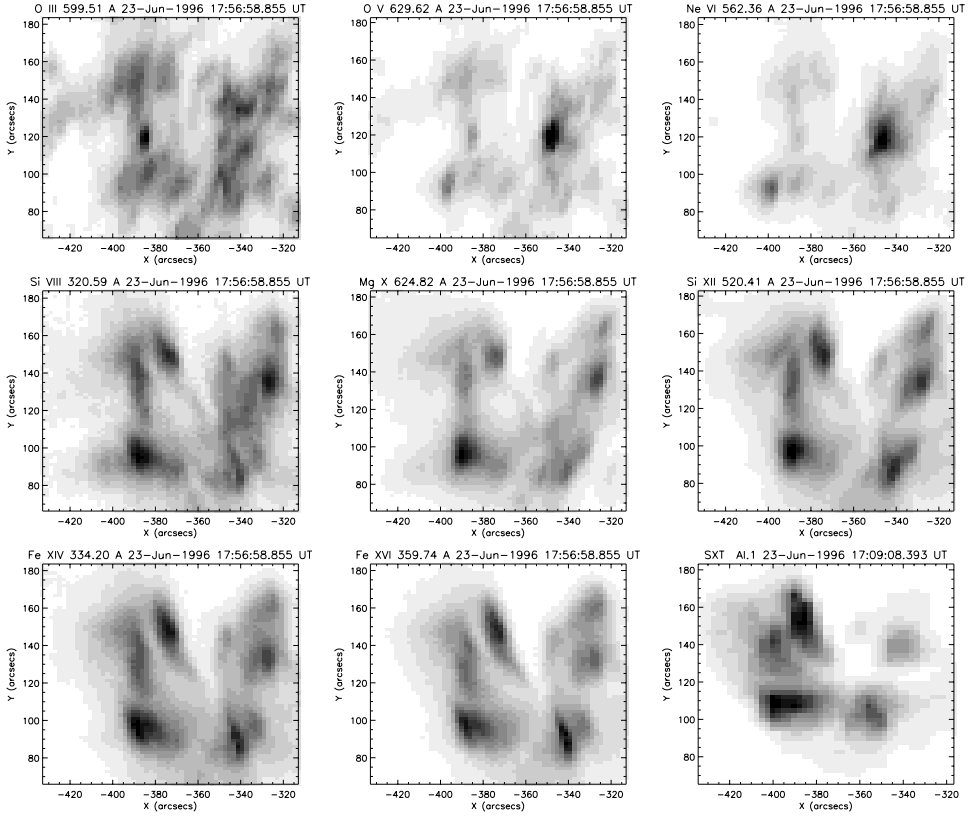

Fig. 1. Intensity maps for AR 7973 in each line observed by CDS, and by SXT through the Al.1 filter. Position from Sun centre is indicated in arcsec along the axes

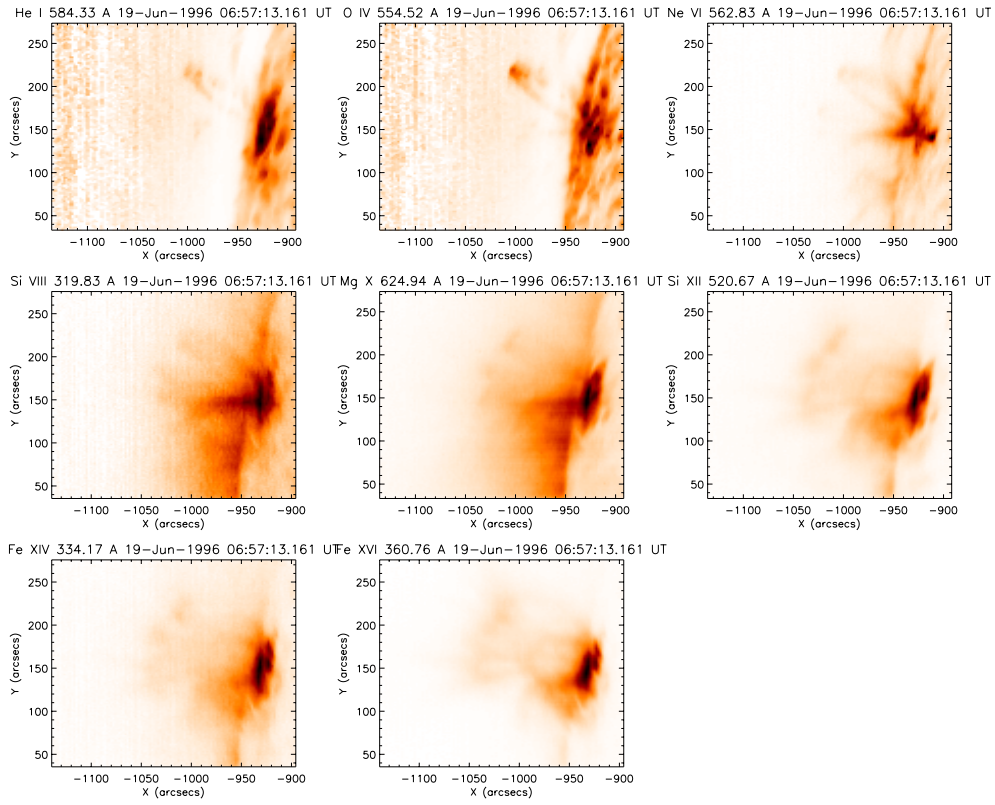

Fig. 2. Intensity maps for AR 7973 observed on the limb in each line observed by CDS. Position from Sun centre is indicated in arcsec along the axes

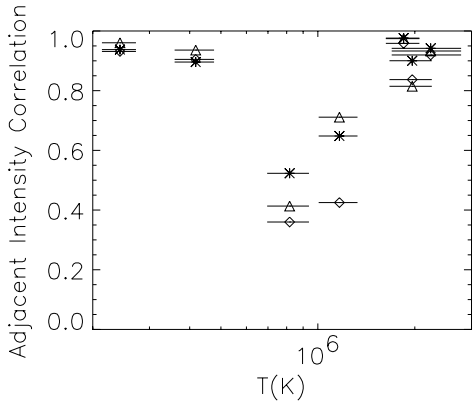

Fig. 3. The variation of the Spearman's correlation coefficient between images of adjacent temperature. Different active regions are represented by the different symbols, * NOAA 8227, △ NOAA 8114, ⋄ NOAA 7973. The error bars are given by the width of the $G(T_e)$ function

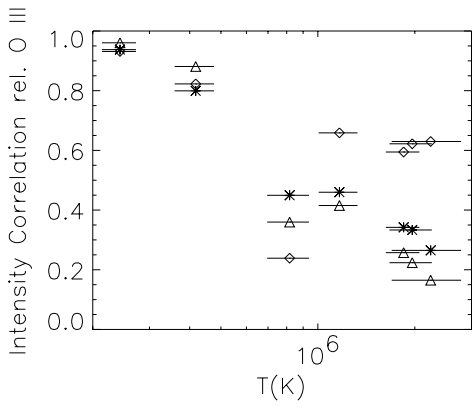

Fig. 4. Similar plot to Fig. 3 showing the correlation relative to O III

formed at all temperatures. The contrast was then defined in the standard way as:

$$\text{contrast} = \frac{\bar{I}_{\rm AR} - \bar{I}_{\rm BG}}{\bar{I}_{\rm AR} + \bar{I}_{\rm BG}}$$

where $\bar{I}_{\rm AR}$ is the average intensity in the chosen active region emission and $\bar{I}_{\rm BG}$ is the average intensity of the background emission in the selected region. Figure 7 shows the variation of the contrast with temperature for the limb observations of NOAA AR 7973 and 7981. The contrast for images formed at low transition region temperatures is high, decreasing sharply from ∼2.2 10^5 K with a minimum being reached at around 1 MK. The contrast then begins to rise again with increasing temperature, although it remains much lower than at TR temperatures. Figure 8 shows the contrast calculated for the regions observed on the disk, AR 7973, 8011, 8122, 8227. For these cases the behaviour is somewhat different from that of the observations on the limb. On disk we find lower values for the cool transition region material than on the limb with a gradual rise in contrast up to ∼4 10^5 K in three out of

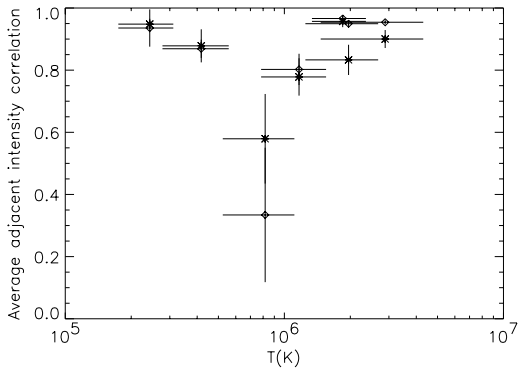

Fig. 5. Disk to limb behaviour of the adjacent intensity correlation with temperature. × represents the average correlation for the first 3 days of the observations beginning at disk centre, while ⋄ represents the average as the region approaches the limb

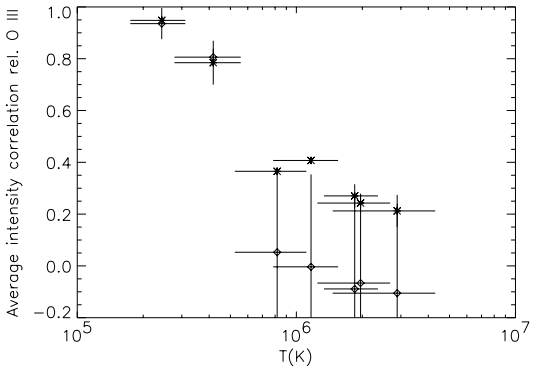

Fig. 6. Disk to limb behaviour of the intensity correlation relative to O III. × represents the average correlation for the first 3 days of the observations beginning at disk centre, while ⋄ represents the average as the region approaches the limb

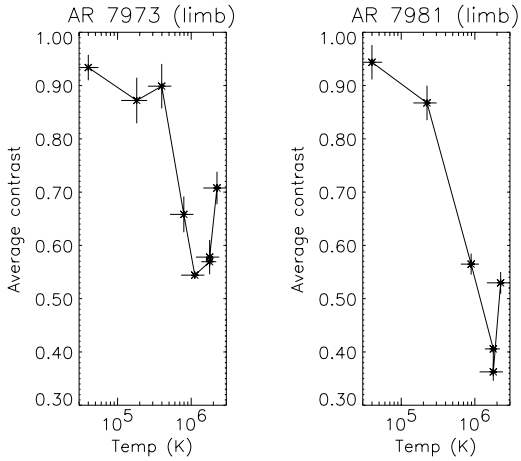

Fig. 7. The variation of the average contrast with temperature for 2 active regions observed on the limb with NIS/CDS

the four regions. A relatively large decrease in contrast then occurs above this temperature, with a minimum at around 6 10^5 K. Similarly to the limb case we then see the contrast begin to rise again at higher temperatures.

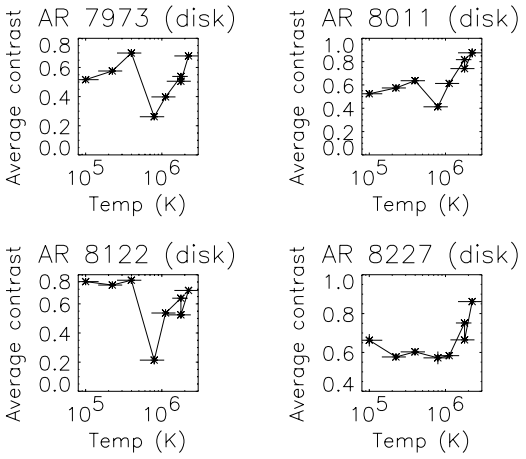

Fig. 8. Variation of average contrast with temperature for the 4 active regions observed on the disk

The limb observations can be easily understood in terms of the relative rarity with which cool structures extend to substantial heights above the solar surface. There is very little overlap of cool loops seen above the limb, and because the diffuse component of the corona is generally hot, the dark background for these loops provides a sharp contrast. Hot loops are very common at all heights, on the other hand, and the overlapping of structures tends to wash out any spatial variability. In addition, the hot diffuse emission between loops raises the level of the background.

The somewhat lower values of contrast seen in the transition region lines on the disk could be due to the still significant contribution of the network at these temperatures. If we look at images in emission lines formed at low transition regions temperatures it is apparent that surrounding them the quiet Sun network is visible (e.g. Fig. 1). The existence of this will tend to raise the level of the defined background emission in our selected rasters, thus reducing the level of the derived contrast. In this case we might expect to see the contrast increase with temperature as the contribution from the network to the background emission decreases, and there is an indication of this in AR 7973 and 8011 but little evidence in ARs 8122 and 8227. The network contrast has its maximum at log $T \simeq 5.4$ with a minimum at log $T = 5.8$ followed by a small increase at temperatures up to log$T \geq 6.0$ where it decreases again (Gallagher et al. 1998). We would then expect to see the contrast in our active regions increase almost monotonically with increasing temperature due to the reduced network contrast at increased temperature, with perhaps a small drop at around log $T = 6.0$. Instead we see a fairly large decrease from log $T = 5.4$ to a minimum at log $T = 5.8$ and then a rise again at higher temperatures. This suggests that the decrease in network contrast cannot completely account for the observed variation.

3.4. Characteristic spatial scales

Improvements in spatial resolution when imaging the corona have consistently shown internal structure down to the limit of that resolution, suggesting that increasingly finer-scale structures will be seen as that resolution improves. The identification of a characteristic spatial scale associated with the structures observed in the EUV and soft X-ray regimes in active regions could provide us with a valuable constraint in terms of determining the possible heating process operating in such a structure. For example, differences in scale with temperature may indicate different physical processes operating in these different temperature regimes, either in terms of the heating process itself or the subsequent transport of the dissipated energy. Fourier methods provide an ideal means of searching for such a characteristic.

Gomez et al. (1993) used data from the Normal Incidence X-ray Telescope (NIXT) to search for evidence of magnetohydrodynamic (MHD) turbulence by using Fourier techniques to examine the spatial distribution of the X-ray intensity within active regions. They looked at several different active regions and found evidence in each case for a power law spectrum of X-ray intensities which fell off with increasing wavenumber as k^{-3}. They suggested that the constancy of this power-law index strongly implied that the same process was generating the X-ray emission in all of the active regions. Martens & Gomez (1992) performed a similar study using data from the Yohkoh SXT. Again they found a broad-band isotropic power-law spectrum for the distribution of X-ray intensities, although with a different power-law index of -2.1 which they attributed to instrumental differences. More recently Berghmanns et al. (1998) have applied the same techniques to quiet Sun data from EIT in the Fe XII and He II bands. In the Fe XII band they found similar broad-band power law behaviour, with a spectral index of -2.52 consistent with the NIXT and SXT results for active regions. However, for the He II they found a spectrum which could not be fitted by a power law and was more consistent with the power spectrum of the solar granulation.

In this work we use the techniques used by Gomez et al. (1993) and apply them to data from the NIS on CDS and SXT on Yohkoh. While it is clear that the spatial resolution of both CDS and SXT is less than optimal, the dataset provides unique tempertaure coverage from 10^5 to $\sim$3 10^6 K and in preforming this analysis we hope to identify whether significant differences can be found in the spatial distribution of EUV and X-ray emission at different temperatures. We performed two-dimensional Fourier transforms for the active regions we observed on the disk (ARs 7973, 8011, 8122, 8227) and then computed the spatial power spectra of the regions. We concentrated on disk regions since projection effects on the limb will tend to introduce a false prevalence of elongated structures. In doing the Fourier transforms we applied standard windowing and zero-padding techniques to minimize the effects of aliasing caused by dealing with finite and non-periodic

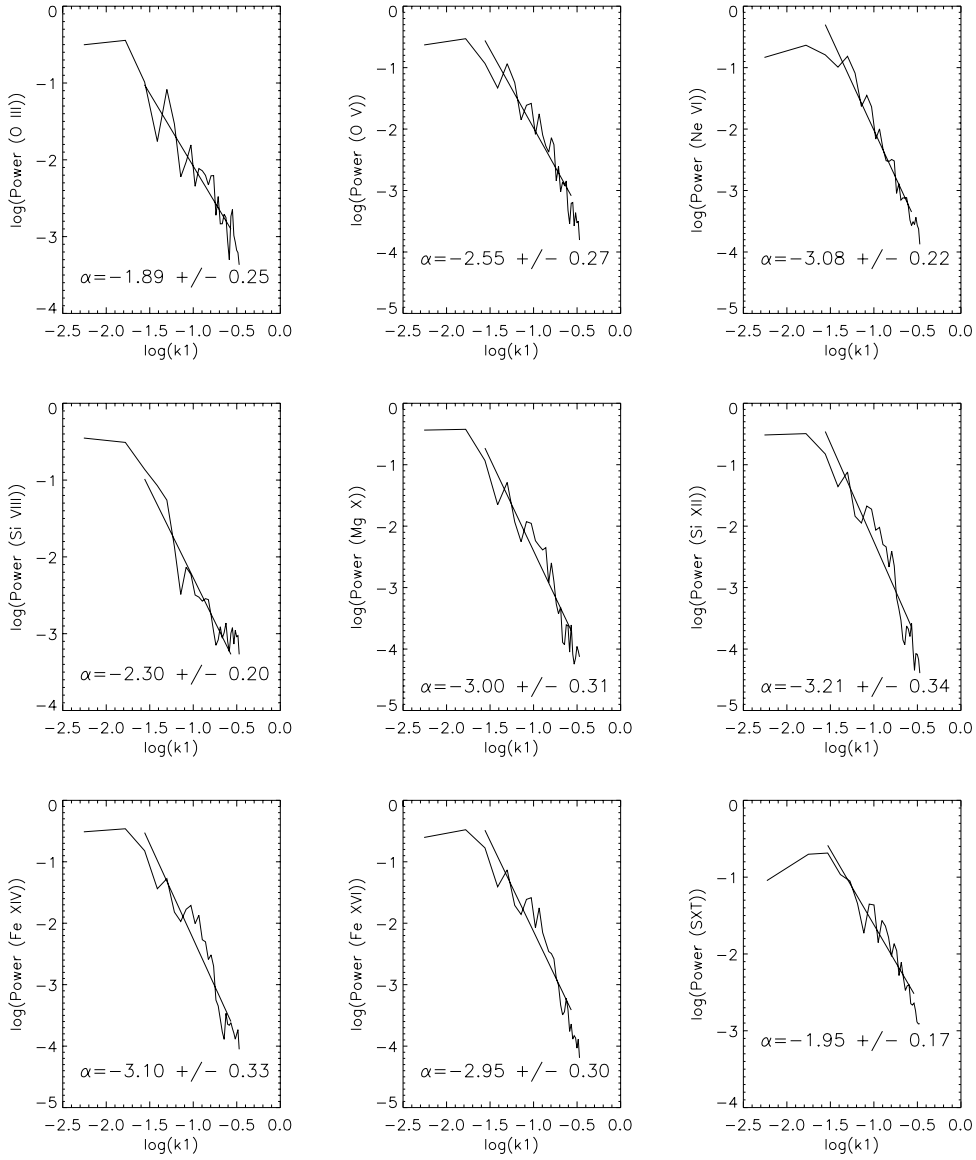

Fig. 9. The omni-directional power spectrum for each temperature line of NOAA AR 7973 at (−350, 130) arcsec from Sun centre

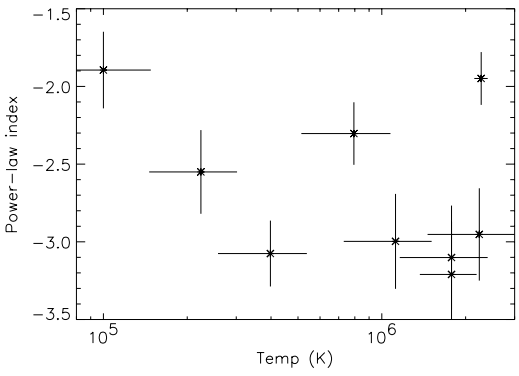

Fig. 10. Variation of the power-law index with temperature for AR 7973

data. The effect of aliasing is to spuriously move wavenumbers outside of the range $-k_c < k < k_c$ (where k_c is the Nyquist critical wavenumber) into that range, thus artificially enhancing the lower modes. Despite these efforts the effects of aliasing were still apparent in our spectra. Since we are dealing with two-dimensional Fourier transforms the definition of the Nyquist wavenumber is not as clear as for the one-dimensional case since our sampling is not uniform. For this reason we have chosen the most conservative Nyquist wavenumber defined by sampling along the diagonal: $k_c = 1/(2 * 1.4) = 0.35$ pixel^{-1}. We minimized edge effects by ensuring that our images of the regions had low intensity at the edges.

The two-dimensional power spectra were found to be isotropic and so we were able to integrate over polar angle

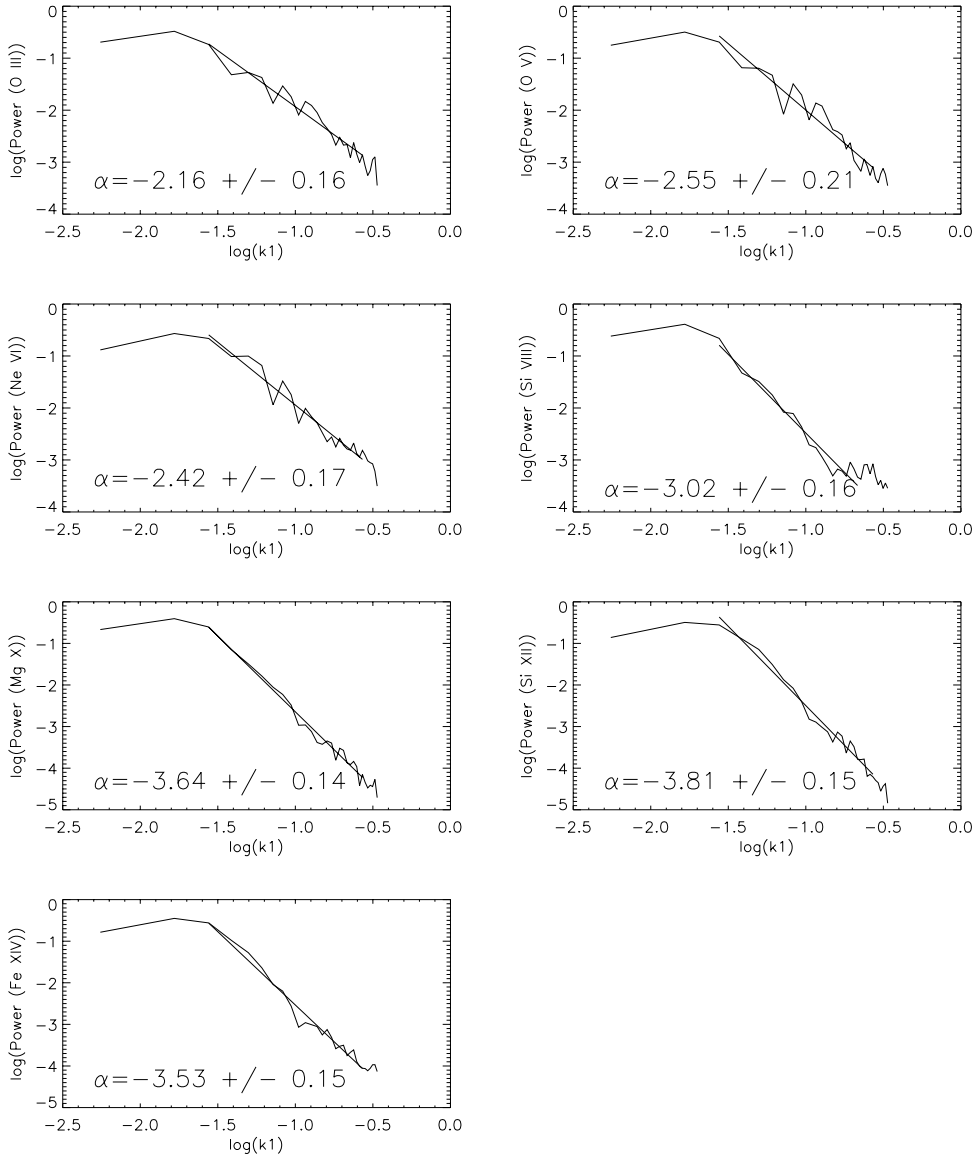

Fig. 11. The omni-directional power spectrum for each temperature line of NOAA AR 8011, at Sun centre

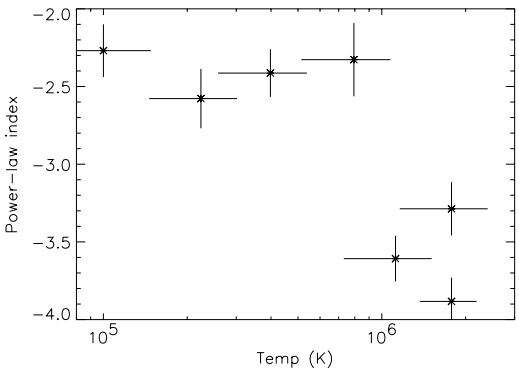

Fig. 12. Variation of the power-law index with temperature for AR 8011

at constant wavenumber to obtain the omni-directional spectrum. This gives us an indication of the existence of any characteristic scales independent of direction,

$$\mathcal{J} = k \int_0^{2\pi} \mathcal{J}_{2\mathrm{D}}(k\cos\theta, k\sin\theta)\mathrm{d}\theta$$

where $\mathcal{J}_{2\mathrm{D}}$ is the 2-D power spectrum and $k = 1/\lambda$ the wavenumber in units of pixel^{-1}.

Figures 9, 11, 13, 15 show the omni-directional power spectra at each temperature for AR 7973, 8011, 8122 and 8227 respectively. The general behaviour in all cases and at all temperatures is that of a power-law spectrum, indicating that there is no preferred length scale within these active regions. However, the existence of aliasing indicates

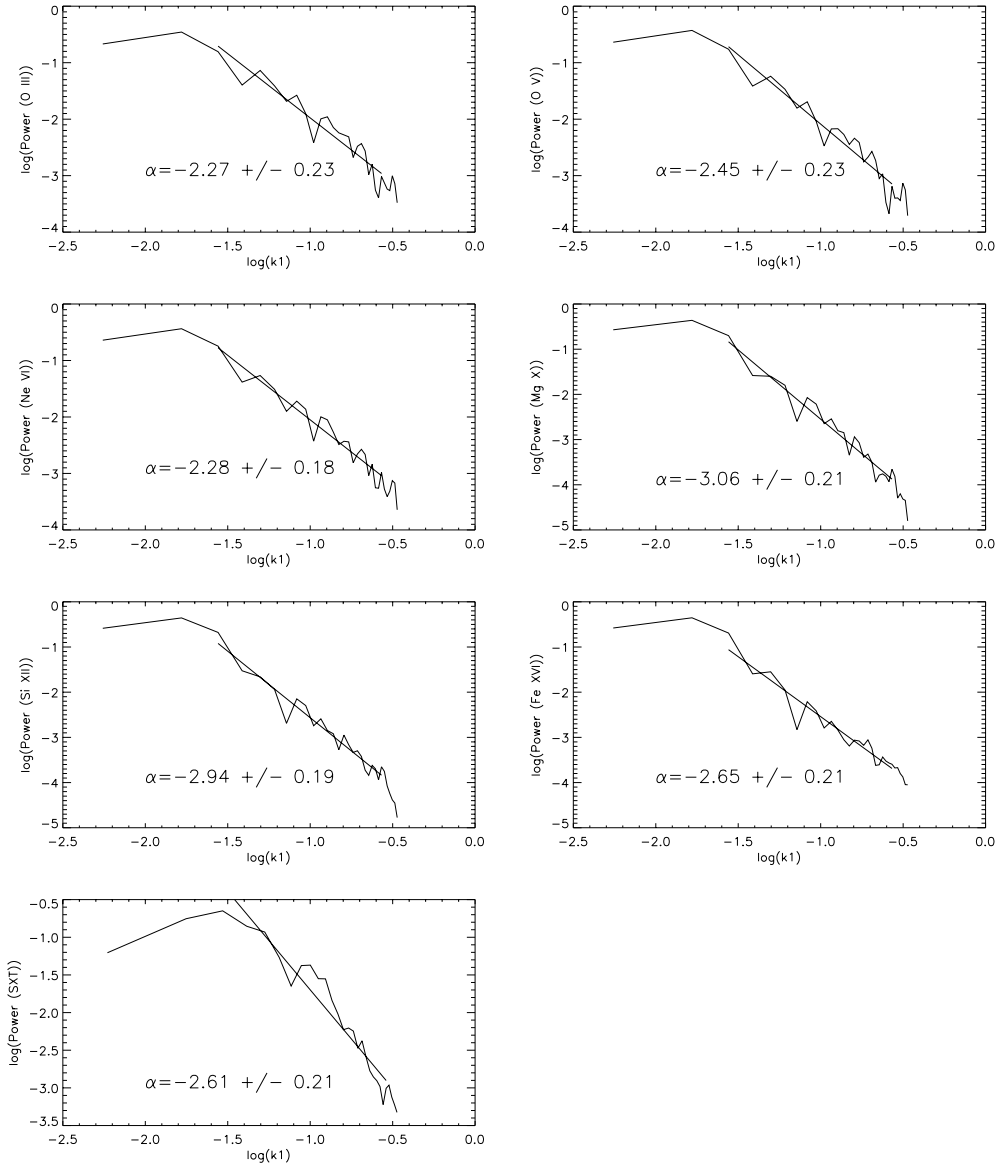

Fig. 13. The omni-directional power spectrum for each temperature line of NOAA AR 8122, at (150, 510) arcsec from Sun centre

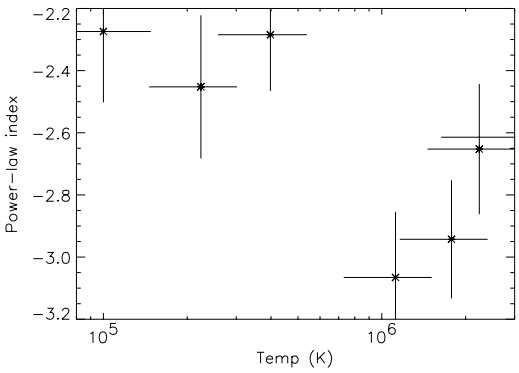

Fig. 14. Variation of the power-law index for AR 8122, with temperature

that there is significant internal structuring below the resolution of our data. Further evidence for this can be seen in images from TRACE at one arcsec resolution. However, we note that power-law behaviour was seen down to 0.75″ resolution with NIXT (Gomez et al. 1993) and therefore we would expect similar behaviour to be seen with TRACE. We fitted the power law spectra obtained for each temperature in each region to determine the best fit spectral index. The spectra were fitted for k values in the range $-1.5 < \log\ k < -0.55$ (note that $\log\ k_c = -0.45$). This range was chosen to exclude those wavelengths comparable to the size of the active region where the power-law ceases to be valid, and those wavelengths where the effects of noise were clear. Although there are cases

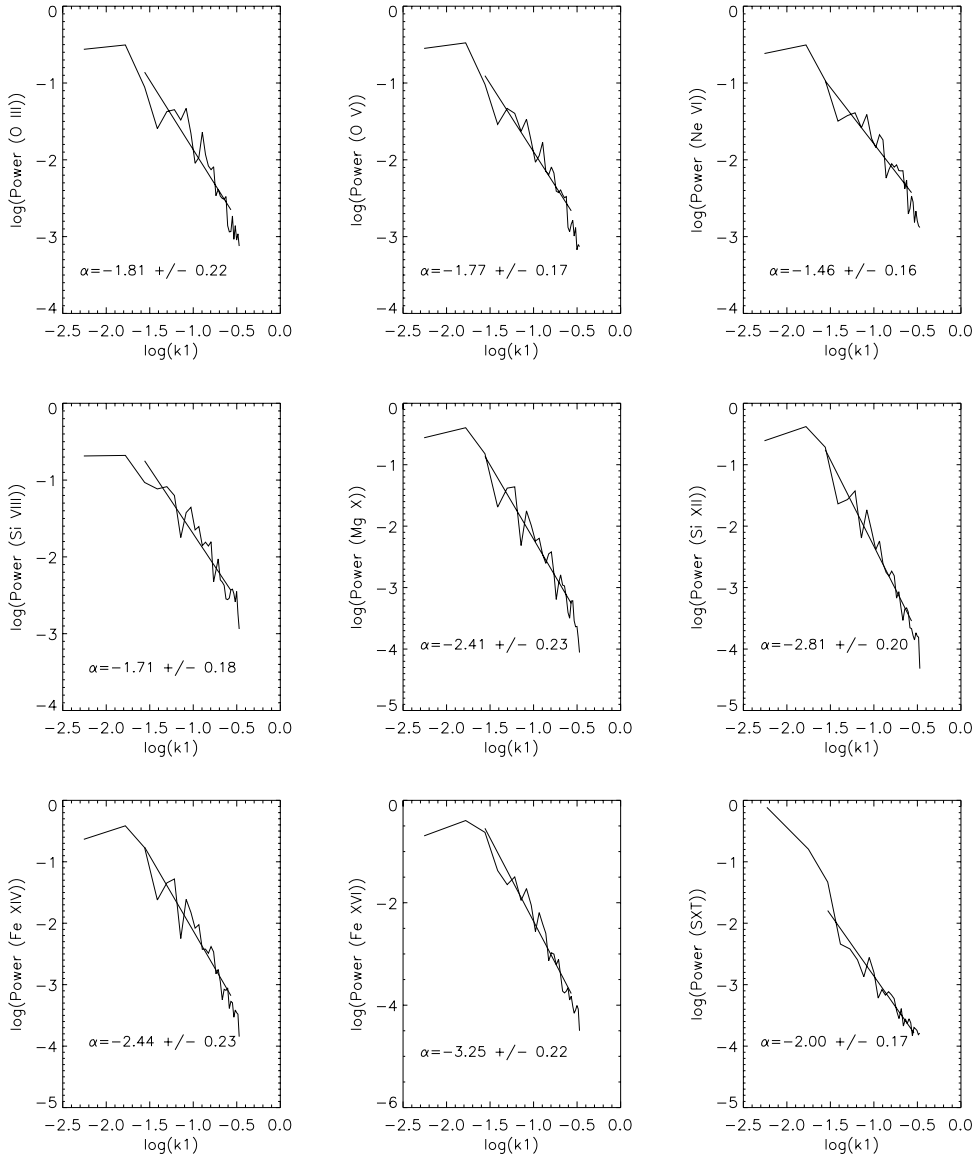

Fig. 15. The omni-directional power spectrum for each temperature line of NOAA AR 8227, at (−60, 430) arcsec from Sun centre

where one might question whether a power-law is the best representation of the spectrum, these were found to provide better fits than exponentials. In Figs. 10, 12, 14, 16 we have plotted spectral index against temperature for each active region in turn. The error bars are from the power-law fit and the *FWHM* of the $G(T_e)$ function. It can be seen that there is a tendency for the spectra to steepen with increasing temperature.

4. Discussion

We have looked quantitatively at several properties of the distribution of different temperature plasma in several topologically different active regions. For all of these active regions we have found similar behaviour irrespective of the overall morphology of the region. When computing

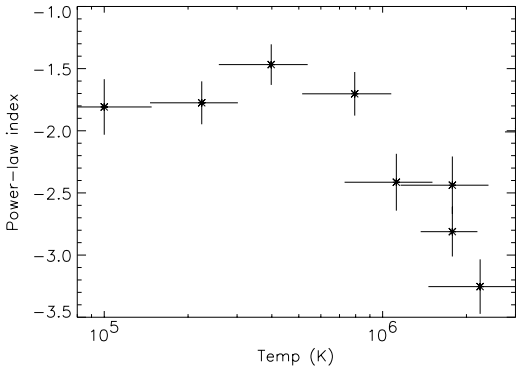

Fig. 16. Variation of the power-law index for AR 8227, with temperature

correlation coefficients between images adjacent in temperature we found high values of the correlation coefficient for $\log T < 5.9$ with a minimum around this temperature, followed by an increase for $\log T > 6.0$. The correlation relative to O III showed a quite different but completely compatible trend with the correlation remaining low for $T > 10^6$ K. This behaviour is also mirrored throughout the passage of AR 8114 across the disk, as can be seen from Figs. 5 and 6. These results agree with those seen in sunspot regions by Brynildsen et al. (1999).

We computed the contrast between loop emission and background emission for two active regions on the limb and found consistently higher contrast at low temperatures, with the change in behaviour occurring somewhere in the range $5.6 < \log T < 5.9$. At temperatures above this we saw the contrast begin to rise again but still remain significantly lower than at transition region temperatures. Contrast on the disk showed different behaviour. While it remained high at low temperatures, it fell sharply from $\log T \simeq 5.8$ and then began to rise again at higher temperatures, reaching similar, if not higher values than at temperatures below $\log T \simeq 5.8$.

For the four topologically different active regions that we have Fourier analysed we have consistently obtained broad-band isotropic power-law spectra over a wide temperature range. The wide temperature coverage of our observations makes this strong evidence for the absence of any preferred spatial scale in active regions. We fitted these omni-directional spectra using cutoffs which corresponded to wavelengths comparable to the size of the active region and where the effect of aliasing and noise became clear. The variation of the best fit power-law index with temperature shows a tendency towards steeper spectra at higher temperatures, indicating an increasing predominance of larger scale structures at higher temperatures.

In order to understand fully how active regions are heated we need not only to be able to find a mechanism that will meet the observed energy requirements, but also to be able to explain the thermal structure of the region. We have seen that a change in behaviour can be found between temperatures of approximately < 5.9 in the log and > 5.9 when we take correlations between intensity maps at adjacent temperatures and relative to the coolest line in our disk studies. This behaviour is seen for four different active regions and appears to be independent of position on the disk. The contrast of loops on the limb and on the disk relative to the background emission also shows a similar difference in these two temperature regimes. It remains low at higher temperatures for regions on the limb and while it increases again with increasing temperature on the disk, in two cases it still never reaches values as high as those observed in the transition region. In terms of standard static loop models the behaviour of the correlations could be understood if we assume that the emission at lower temperatures comes from a combination of cool loops and the footpoints of hot loops. In this case we would expect only limited correlation with hotter emission. If the emission in the intermediate temperature range, $\log T = 5.9$–6.0, comes exclusively from the footpoints of hot loops, and the emission hotter than this from the coronal parts of the loops, then again we would expect little correlation with hotter material for the intermediate range.

The existence of broad-band power-law spectra at all temperatures in topologically different active regions indicates that there is no preferred size scale for this emission, although as discussed above the existence of aliasing indicates the presence of significant struture below the limits of our resolution. With greater spatial resolution a peak in the power at smaller size scales may become apparent. However, we note that at the $0.75''$ resolution of NIXT power-law spectra are still seen. It has been suggested that the existence of these power-law spectra indicates that turbulence plays a role in determining the structure and ultimately the heating of the corona (e.g. Gomez et al. 1993; Martens & Gomez 1992; Benz et al. 1997; Berghmanns et al. 1998). Hollweg (1983) suggested that kinetic energy injected over large scales by sub-photospheric convective motions might cascade down through non-linear interactions to scales where viscosity and resistivity could produce effective dissipation. In Fourier terms this translates into a broad-band isotropic spectrum with energy injected at low wavenumbers and the dissipation region at high wavenumbers. The region between, the inertial regime, is dominated by non-linear interactions, and this region is characterized by the power-law index. However, even if turbulence develops in the corona itself, the intertial regime is likely to begin near the smallest observable scales and extend to sub-resolution sizes; most of the observed spectrum is outside of this range. Also, it is not obvious how the kinetic energy density spectrum of the turbulent eddies is related to the power spectrum of the resulting emission pattern. Thus, while we believe that the differences in the power-law indices at different temperatures may indicate differences in the heating at these temperatures, we are reluctant to conclude, as others have, that the existence of power-laws themselves provides evidence for turbulent heating.

Our results show that the steepness of the omni-directional spectra changes with temperature, becoming steeper at higher temperatures. The enhanced power at high wavenumbers for low temperatures could be consistent with the bulk of this emission originating in low-lying loops and the footpoints of hotter loops. What this, together with the results for the intensity correlations and contrast, are almost certainly telling us is that the transition region is made up of several components. It appears, when the results of this study are considered in parallel to other investigations, that there are indeed real physical differences between these different temperature plasmas which must be taken into account when modelling potential heating processes. The finer scale structure, sharper contrast and more dynamic behaviour of the cooler plasma

suggests a very high degree of both spatial and temporal intermittency in the heating of these structures. The suggestion by Schrijver at al. (1999) that the apparent reduction in contrast with increasing temperature observed by TRACE is in fact due to an increase in filling factor with temperature could be consistent with the possibility that different types of energy release may be occurring. We might expect that a spatially and temporally intermittent energy release process would lead to smaller filling factors than a more homogeneous mechanism.

Acknowledgements. LKH would like to thank PPARC for an Advanced Fellowship. The work of JAK was funded by the NASA Sun-Earth Connections GI program. We would like to thank M. Blackman for many useful discussions on Fourier analysis, S. Antiochos for helpful discussions and the referee for helping to greatly clarify the manuscript.

References

Athay, R. G., Gurman, J. B., Henze, W., & Shine, R. A. 1983, ApJ, 265, 519
Benz, A. O., Krucker, S., Acton, L. W., & Bastian, T. S. 1997, A&A, 320, 993
Berger, T. E., De Pontieu, B., Fletcher, L. et al. 1999, Solar Phys., 190, 409
Berghmanns, D., Clette, F., & Moses, D. 1998, A&A, 336, 1039
Brosius, J. W., Davila, J. M., Thomas, R. J., et al. 1997, ApJ, 477, 969
Brynildsen, N., Maltby, P., Brekke, P., Haugan, S. V. H., & Kjeldseth-Moe, O. 1999, Solar Phys., 186, 141
Cheng, C.-C. 1980, ApJ, 238, 743
Cheng, C.-C., Smith, J. B., & Tandberg-Hanssen, E. 1980, Solar Phys., 67, 259-265
Dere, K. P. 1982, Solar Phys., 75, 189-203, 105, 35
Fludra, A., Brekke, et al. 1999, Solar Phys., 190, 409; 1997, Solar Phys., 175, 487
Gallagher, P. T., Phillips, K. J. H., Harra-Murnion, L. K., & Keenan, F. P. 1998, A&A, 335, 733
Gomez, D., Martens, P. C. H., & Golub, L. 1993, ApJ, 405, 767
Hara, H. 1996, Ph.D. Thesis, National Astronomical Observatory
Harrison, R. A., et al. 1995, Solar Phys., 162, 233-290
Hollweg, J. V. 1983, Solar Wind V, NASA Conf. Publ. 2280, 5, ed. M. Neugebauer
Martens, P. C. H., & Gomez, D. 1992, PASJ, 44, L187
Martens, P. C. H., Kankelbourg, C., & Berger, T. 1999, ApJ, submitted
Mariska, J. T., Feldman, U., & Doschek, G. A. 1980, ApJ, 240, 300
Matthews, S. A., & Harra-Murnion, L. K. 1997, Solar Phys., 175, 541
Nagata, S., Hara, H., Kano, et al. 1999, ApJ, submitted
Pauluhn, A., Ruedi, I., Solanki, S., et al. 1999, Appl. Opt., 38, 7035
Press, W. H., Teukolsky, S. A., Vetterling, W. T., & Flannery, B. P. 1992, Numerical Recipes in C: The Art of Scientific Computing (Cambridge University Press)
Schrijver, C., et al. 1999, Solar Phys., 187, 261
Sheeley, N. R. 1980, Solar Phys., 66, 79
Strong, K. T., & Bruner, M. E. 1996, Adv. Space Res., 17, 4/5, 179-188
Webb, D. F. 1981, Solar Active Regions: A Monograph from Skylab Solar Workshop III, Colorado (Associated University Press), 165